

2.5D REVERSE TIME MIGRATION

F.A. da Silva Neto, J.C. Costa, J. Schleicher, and A. Novais

email: *jesse@ufpa.br*

keywords: *reverse time migration, 2.5D, finite-difference, seismic imaging*

ABSTRACT

Reverse time migration (RTM) in 2.5D offers an alternative to improve resolution and amplitude when imaging 2D seismic data. Wave propagation in 2.5D assumes translational invariance of the velocity model. Under this assumption and using velocity-pressure for the acoustic wavefield we implemented a finite difference modelling algorithm in the mixed time-space/wavenumber domain. The algorithm is truly parallel, which allows an efficient implementation in clusters. Storage and computing time requirements are reduced compared to a full 3D FD simulation of the wave propagation. This feature make 2.5D RTM much more efficient than 3D RTM. Reverse time migration in 2.5D correctly models the geometrical spreading and the phase of the seismic waveform. This brings the possibility to recover amplitudes proportional to the earth's reflectivity using an imaging condition that compensates for uneven illumination and/or the obliquity factor. Numerical experiments using synthetic data demonstrate the better resolution and amplitude recovery of 2.5D RTM relative to 2D reverse time migration.

INTRODUCTION

The computational demand for 3D pre-stack reverse time migration (RTM) is high compared to wave equation migration by downward extrapolation of the wavefield (Biondi, 2006). However, low cost parallel computing and more efficient storage hardware is making RTM feasible. The difficulties of imaging steeply dipping reflectors and complex structures in complicated velocity models, for example below salt bodies, has created the need for a migration method that models wave propagation in such media accurately. Reverse-time migration is the best known method capable of handling this challenge.

Additionally to its superior imaging capabilities, advances have been made in amplitude preservation in RTM. Several attempts to improve the amplitudes in RTM are based on illumination compensation with different kinds of stabilisation (Valenciano and Biondi, 2003; Kaelin and Guitton, 2006). Attempting to better understand the amplitudes in RTM, Haney et al. (2005) performed an asymptotic analysis of the cross-correlation imaging condition. Their analysis assumes a single planar reflector in a 3D homogeneous medium, full coverage, and infinite aperture. They demonstrate that the amplitudes of RTM are affected by an obliquity factor that depends on the reflector dip. Most recently, Chattopadhyay and McMechan (2008) explicitly compared the imaging conditions most commonly used in practice to make clear which are viable for recovering accurate amplitudes and which are not.

Based on the result of Haney et al. (2005), Costa et al. (2009) propose a new imaging condition for amplitude preservation in RTM. The idea is to asymptotically correct for obliquity factor by introducing a weight factor in the source-normalised imaging condition. They also report an improvement of the images when the obliquity factor is included together with illumination compensation in the imaging condition for RTM.

However, there is a problem with amplitude recovery in RTM for the case of seismic data acquired on a single line. In this situation, application of RTM generally relies on 2D wave extrapolation techniques. This will harm the efforts to extract meaningful amplitudes since the geometrical-spreading effects of 3D

wave propagation are incorrectly simulated. A possible solution to this problem is to extend the model to three dimensions under the assumption of translation invariance and then simulate the wave propagation using 3D techniques. For many applications, however, this procedure is unacceptably expensive, particularly for its storage requirements. A cheaper solution is the use of 2.5D techniques, which explore the medium symmetry to simulate full 3D wave propagation. While 2.5D descriptions of wave propagation are straightforward for ray-based solutions (Bleistein, 1986), such modifications for the finite-difference (FD) method have not been available until recently (Novais and Santos, 2005; Costa et al., 2005). As shown in their works, 2.5D FD simulates wave propagation with the same quality as 3D FD with a reduced computational cost and storage requirements corresponding to 2D FD. Moreover, 2.5D FD is an embarrassingly parallel process that can be efficiently implemented on clusters.

In this work, we demonstrate the application of 2.5D FD methods in RTM. The same conclusions regarding computational cost and storage requirements also apply to 2.5D RTM. Numerical experiments demonstrate the superior quality of 2.5D RTM images as compared to their 2D counterparts.

METHODOLOGY

As any 2.5D technique, also 2.5D RTM migration assumes the medium to be translation invariant in the direction perpendicular to the seismic line. It relies on 2.5D FD, which explores this symmetry of the velocity model to simplify the simulation of full 3D wave propagation. Below, we give a brief introduction to the 2.5D FD method.

Using index notation and summation convention, the system of equations that governs the acoustic wavefield in 3D is

$$\begin{aligned}\rho(\mathbf{x}) \frac{\partial v_j(\mathbf{x}, t)}{\partial t} &= -\frac{\partial p(\mathbf{x}, t)}{\partial x_j} + f_j(\mathbf{x}, t); \\ \frac{\partial p(\mathbf{x}, t)}{\partial t} &= -\rho(\mathbf{x})c^2(\mathbf{x}) \frac{\partial v_j(\mathbf{x}, t)}{\partial x_j} + \frac{\partial q(\mathbf{x}, t)}{\partial t}; \quad (j = 1, 2, 3); \end{aligned} \quad (1)$$

where ρ is the medium mass density, c is the propagation velocity, v_j and p are the velocity and pressure wavefields, f_j represents a dipole source and q the rate of injection of an explosive source.

Let the direction of translational invariance of the medium be denoted by the x_2 coordinate. Because the medium properties are independent of x_2 , it is then convenient to apply a Fourier transform in that direction to the acoustic wavefield, viz.,

$$v_j(\mathbf{x}, t) = \int_{-\infty}^{\infty} V_j(\mathbf{X}, k_2, t) \exp(ik_2x_2) dk_2, \quad (2)$$

and

$$p(\mathbf{x}, t) = \int_{-\infty}^{\infty} P(\mathbf{X}, k_2, t) \exp(ik_2x_2) dk_2, \quad (3)$$

where k_2 is the wavenumber associated with x_2 and $\mathbf{X} \equiv (x_1, x_3)$. Moreover, $V_j(\mathbf{X}, k_2, t)$ and $P(\mathbf{X}, k_2, t)$ denote the complex valued components of the acoustic wavefield in the mixed (\mathbf{X}, k_2, t) -domain. The source distributions q and f_j can be represented in a similar way in using their counterparts Q and F_j , respectively, in this domain.

The components of the acoustic wavefield and its source distributions are solution of the complex-valued system

$$\begin{aligned}\rho(\mathbf{X}) \frac{\partial V_J}{\partial t} &= -\frac{\partial P}{\partial X_J} + F_J \\ \rho(\mathbf{X}) \frac{\partial V_2}{\partial t} &= -ik_2 P + F_2 \\ \frac{\partial P}{\partial t} &= -\rho(\mathbf{X})c^2(\mathbf{X}) \left(\frac{\partial V_J}{\partial X_J} + ik_2 V_2 \right) + \frac{\partial Q}{\partial t} \end{aligned} \quad (4)$$

where the index J assumes only the values 1 and 3.

We assume the source distributions have specular symmetry with respect to the x_1 - x_3 plane. This symmetry implies:

- 1- the dipole source component in the x_2 direction vanishes, i.e., $f_2 = 0$;
- 2- the velocity components $v_J(\mathbf{x}, t)$ are an even functions of x_2 and, thus, their Fourier transforms $V_J(\mathbf{X}, k_2, t)$ are real-valued quantities;
- 3- the velocity component $v_2(\mathbf{x}, t)$ is an odd function of x_2 and, thus, its Fourier transform $V_2(\mathbf{X}, k_2, t)$ is a pure imaginary quantity.

Defining $U_2(\mathbf{X}, k_2, t) \equiv iV_2(\mathbf{X}, k_2, t)$, the acoustic wavefield in the mixed space/wavenumber domain satisfies the real-valued system

$$\begin{aligned} \rho(\mathbf{X}) \frac{\partial V_J}{\partial t} &= -\frac{\partial P}{\partial X_J} + F_J, \\ \rho(\mathbf{X}) \frac{\partial U_2}{\partial t} &= k_2 P, \\ \frac{\partial P}{\partial t} &= -\rho(\mathbf{X}) c^2(\mathbf{X}) \left(\frac{\partial V_J}{\partial X_J} + k_2 U_2 \right) + \frac{\partial Q}{\partial t}. \end{aligned} \quad (5)$$

The numerical solution of this system of equations by finite differences is discussed in Costa et al. (2005). After solving this system of equations, the acoustic wavefield in the space-time domain can be computed from

$$v_J(x_1, x_2, x_3, t) = \frac{1}{2\pi} \int_{-\infty}^{+\infty} V_J(x_1, k_2, x_3, t) e^{ik_2 x_2} dk_2 \quad (6)$$

$$v_2(x_1, x_2, x_3, t) = -\frac{i}{2\pi} \int_{-\infty}^{+\infty} U_2(x_1, k_2, x_3, t) e^{ik_2 x_2} dk_2 \quad (7)$$

and

$$p(x_1, x_2, x_3, t) = \frac{1}{2\pi} \int_{-\infty}^{+\infty} P(x_1, k_2, x_3, t) e^{ik_2 x_2} dk_2. \quad (8)$$

The algorithm represented by this set of equations requires the solution of an independent 2D FD system of equations in the (\mathbf{X}, t) -domain for each wavenumber k_2 . This can be implemented very efficiently in a parallel architecture with each value of k_2 being assigned to a different processing unit.

We use this algorithm to implement RTM in 2.5D. For each common-shot gather the source wavefield is propagated forward in time. Afterwards, the receiver wavefield is backpropagated in time and the imaging condition is applied at every time step. The final migrated image is the stack of all common shot images.

The cross-correlation imaging condition for shot-profile migration reads (Claerbout, 1985)

$$I(\mathbf{x}) = \sum_{\mathbf{x}_s} \sum_{\mathbf{x}_g} \int_0^{t_{max}} p_s(\mathbf{x}, t; \mathbf{x}_s) p_g(\mathbf{x}, t; \mathbf{x}_g) dt. \quad (9)$$

It produces an image, $I(\mathbf{x})$, by cross-correlating two wavefields with zero temporal and spatial lag. The two wavefields are $p_s(\mathbf{x}, t; \mathbf{x}_s)$, which represents the forward propagated wavefield from the source, \mathbf{x}_s , to the image point, \mathbf{x} , and $p_g(\mathbf{x}, t; \mathbf{x}_g)$, which represents the receiver wavefield that is backpropagated in reverse time from the receiver, \mathbf{x}_g , to the image point. Here, t_{max} is maximum recorded time.

The cross-correlation imaging condition (9) does not take into account other issues that may affect the resulting amplitude when applying RTM in complex velocity models, like the lack of full coverage of sources and receivers and the uneven illumination of the targets. Illumination compensation is achieved normalising the cross-correlation imaging condition by the source energy at the imaging point (Biondi, 2006)

$$I(\mathbf{x}) = \int_{\mathbf{x}_s} \frac{\int_{\mathbf{x}_g} \int_0^{t_{max}} p_s(\mathbf{x}, t; \mathbf{x}_s) p_g(\mathbf{x}, t; \mathbf{x}_g) dt d\mathbf{x}_g}{\int_0^{t_{max}} p_s(\mathbf{x}, t; \mathbf{x}_s) p_s(\mathbf{x}, t; \mathbf{x}_s) dt} d\mathbf{x}_s. \quad (10)$$

However, condition (10) is known to enhance migration artifacts. An improved imaging condition combines the illumination compensation with an obliquity factor weight function in the imaging condition

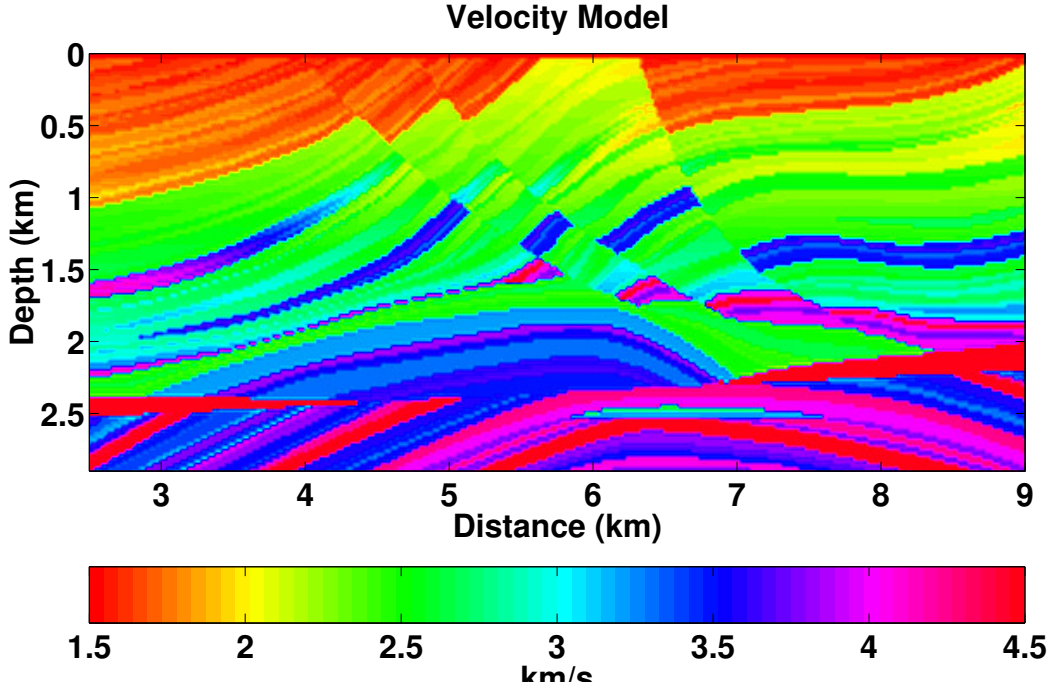


Figure 1: Marmousi velocity model. The dark red high-velocity zones in the lower part of the model represent salt intrusions.

(Costa et al., 2009)

$$I(\mathbf{x}) = \int_{\mathbf{x}_s} \frac{\int_{\mathbf{x}_g} \int_0^{t_{max}} W(\mathbf{S}_s, \mathbf{S}_g) p_s(\mathbf{x}, t; \mathbf{x}_s) p_g(\mathbf{x}, t; \mathbf{x}_g) dt d\mathbf{x}_g}{\int_0^{t_{max}} p_s(\mathbf{x}, t; \mathbf{x}_s) p_s(\mathbf{x}, t; \mathbf{x}_s) dt} d\mathbf{x}_s, \quad (11)$$

where \mathbf{S}_s represents the Poynting vector of the source wavefield and \mathbf{S}_g represents the Poynting vector of the receiver wavefield. The weight function consists of two independent factors

$$W(\mathbf{S}_s, \mathbf{S}_g) = \cos^3 \alpha \cos^3 \theta, \quad (12)$$

where $\cos^3 \alpha$ is the obliquity compensation factor and $\cos^3 \theta$ is a scattering angle taper. Both factors can be applied individually or jointly. Both the scattering angle θ and the propagation angle α can be determined from Poynting-vector information. The scattering angle θ is given by

$$\cos^2 \theta = \frac{1}{2} \left(1 + \frac{\mathbf{S}_s \cdot \mathbf{S}_g}{\|\mathbf{S}_s\| \|\mathbf{S}_g\|} \right), \quad (13)$$

and the propagation angle α , i.e., the angle between the bisection of the propagation directions and the vertical, by

$$\cos \alpha = \begin{pmatrix} 0 \\ 0 \\ 1 \end{pmatrix} \cdot \left(\frac{\mathbf{S}_s}{\|\mathbf{S}_s\|} + \frac{\mathbf{S}_g}{\|\mathbf{S}_g\|} \right) / \left\| \left(\frac{\mathbf{S}_s}{\|\mathbf{S}_s\|} + \frac{\mathbf{S}_g}{\|\mathbf{S}_g\|} \right) \right\|. \quad (14)$$

When applied together with the 2.5D simulation of 3D wave propagation, these imaging conditions will help to improve the amplitude recovery from the migration of 2D seismic data using RTM.

NUMERICAL EXPERIMENTS

We evaluate the 2.5D RTM technique discussed above using the Marmousi synthetic data set (Billette et al., 2003). This data set was simulated using the ray-Born approximation in 2.5D. The velocity model for

raytracing is a smoothed version of the original Marmousi velocity model (see Figure 1). The absence of multiples and the correct computation of 3D geometrical spreading makes this synthetic data set the ideal benchmark for the first test of our 2.5D RTM algorithm. The data set consists of 261 common-shot gathers with 96 receivers per shot, regularly spaced at 25 m. The nearest offset is 100 m. The recording time is 3 s with a 4 ms sampling interval.

The velocity model is defined on a regular mesh with 485 nodes in the vertical direction and 1533 nodes in the horizontal direction. Node spacing is 6 m. The source wavefield was simulated using a Blackman-Harris wavelet with a peak frequency of 30 Hz.

Experiment without illumination compensation

Figures 2 and 3 compare the results of 2D and 2.5D RTM using the cross-correlation imaging condition of equation (9). The most eye-popping difference between these images is their amplitude behaviour. The events in the 2D migrated image have a much smaller amplitude variation from top to bottom when compared to the 2.5D migrated image. This feature reflects the difference in the geometrical-spreading factor between the 2D and 3D propagation. The geometrical spreading for 2D propagation is much smaller than that for 3D.

While the 2D amplitude behaviour actually might be desirable, there is another remarkable difference between the 2D and 2.5D images with respect to resolution. It is evident from Figures 2 and 3 that the 2.5D migrated image has a better resolution than the 2D image. Note that the events in the central part of the model, the limits of the faults, and the thin layers are much better defined. A more detailed analysis also reveals phase difference between the pulses, namely a symmetric pulse for the 2.5D RTM and a nonsymmetric pulse for 2D RTM. The reason for both the differences in resolution and phase is that 3D propagation simulates a point source while 2D propagation simulates a line source. Line sources add a phase rotation and a half-derivative to the source pulse, while point sources add a full derivative and no phase rotation. Thus 2.5D RTM preserves a higher frequency content of the wavelet.

Experiment with illumination compensation

The second numerical experiment uses the image condition (10) with amplitude compensation. Figures 4 and 5 show the results of 2D and 2.5D RTM, respectively.

The illumination compensation resulted in a good equalisation of the amplitudes in both images for most of the events and eliminate the strong amplitude differences between the images. However, more subtle amplitude differences are still noticeable, particularly in the lower left portion of the images below 2000 m. The 2.5D RTM image presents larger differences between the amplitudes of different reflectors. This behaviour is in agreement with the reflectivity in this area. The strongest impedance contrast, i.e., that between the sediments and the salt intrusions (see again Figure 1 has the highest amplitudes. Moreover, the illumination compensation strongly highlights the difference in resolution of between 2.5D and 2D RTM. This is clearly visible in the whole images, but particularly in the region between 5000 m-8000 m.

In conclusion, our numerical experiments indicate that 2.5D RTM has a very beneficial effect on image resolution. Moreover, when combined with illumination compensation, it also helps to improve amplitude recovery. Whenever these features are critical in an imaging project of 2D seismic data, the additional computational cost of 2.5D RTM over 2D RTM is justified.

CONCLUSIONS

We implemented 2.5D RTM and evaluated our algorithm using the Marmousi synthetic data set. The underlying 2.5D modelling algorithm consists of a sequence of independent 2D finite difference modelling steps in the mixed time-space/wavenumber domain. This characteristic makes the forward problem a truly parallel algorithm and its implementation very efficient in parallel architectures. In this way, the computational cost of 2.5D RTM is that of 2D RTM times the number of out-of-plane wavenumbers that need to be used, divided by the number of processing units available. The second and most important feature of 2.5D RTM is its low memory demand when compared to a 3D implementation, since only 2D snapshots need to be stored during the process.

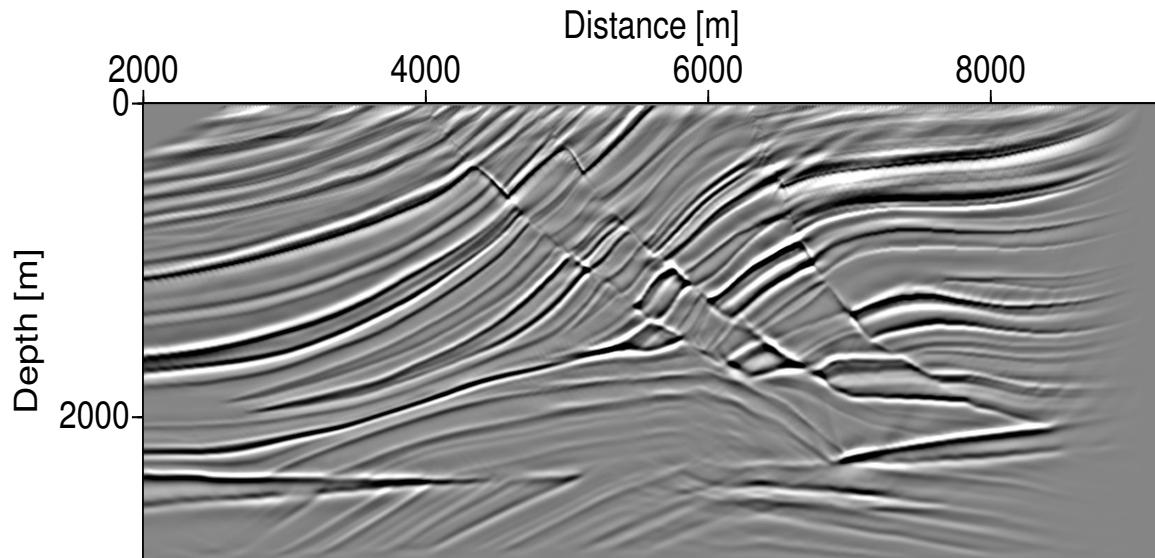


Figure 2: 2D RTM image computed cross-correlation imaging condition (9).

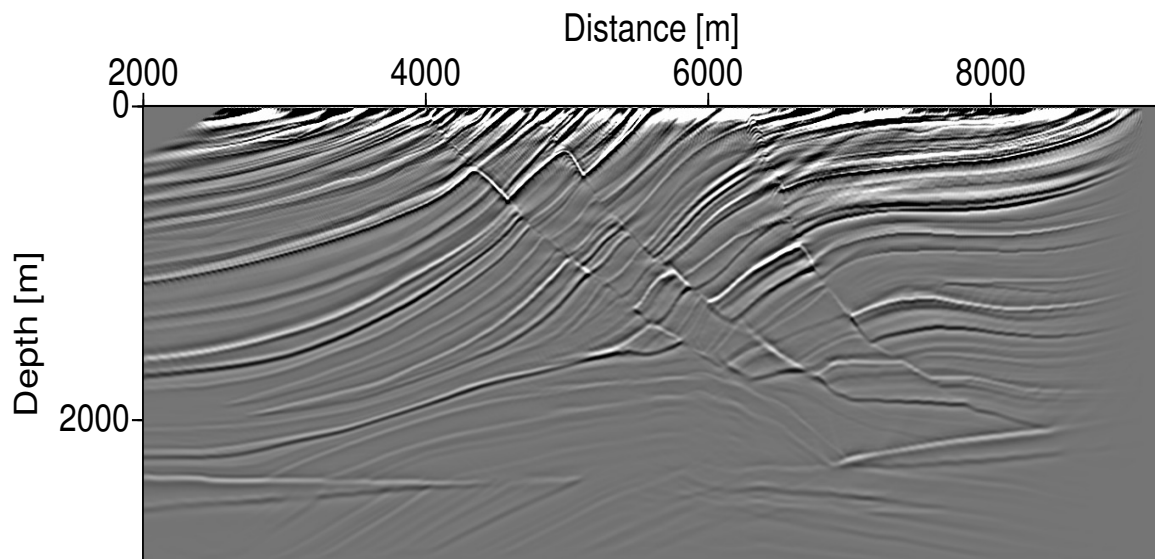


Figure 3: 2.5D RTM image computed cross-correlation imaging condition (9).

Our numerical experiments show the improved quality of 2.5D RTM images when compared to their 2D counterparts. The main advantage of 2.5D RTM is its higher resolution. This improves the delineation of subtle features in the image, as for example, faults and thin-layer boundaries. When combined with illumination compensation imaging conditions, our 2.5D RTM images also provided a clear improvement of amplitudes such that the resulting RTM amplitude variations were correlated to reflectivity changes. These improvements are sufficiently significant to justify the higher computational cost of 2.5D RTM whenever these features are critical to the success of an imaging project.

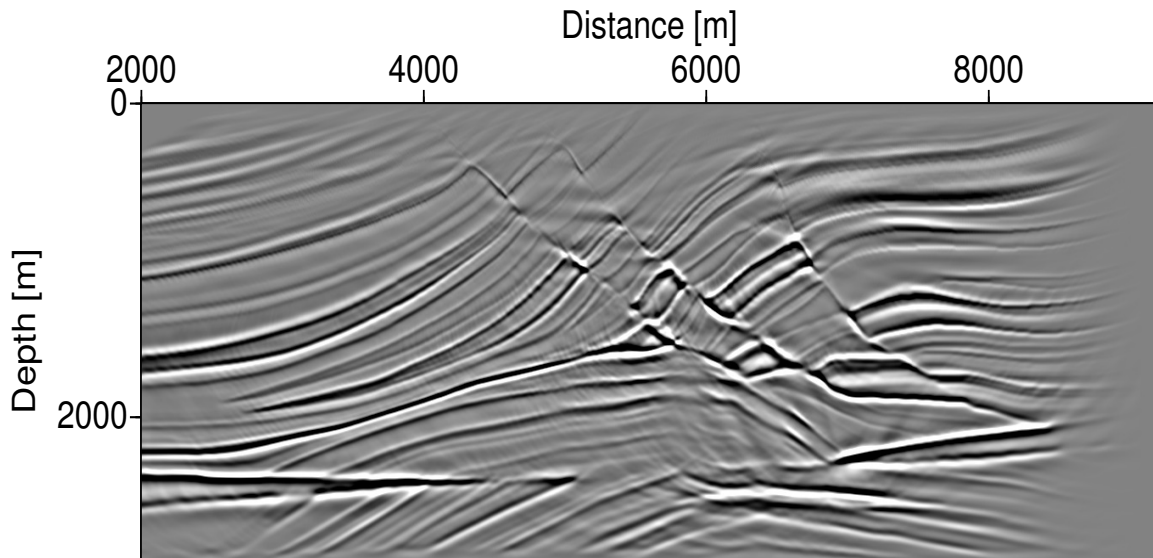


Figure 4: 2D RTM image computed with illumination compensation using imaging condition (10).

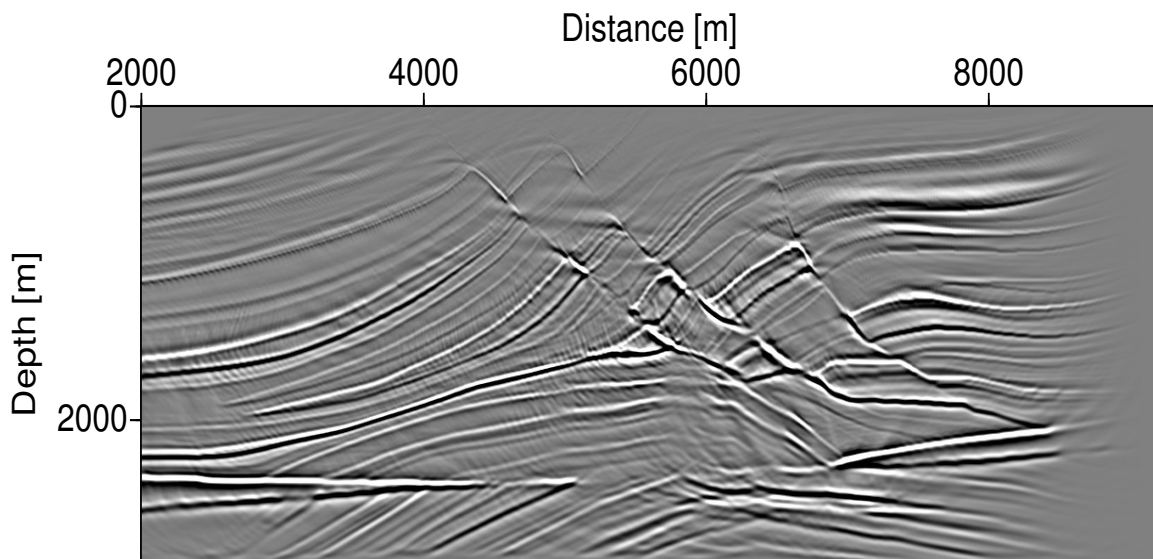


Figure 5: 2.5D RTM image computed with illumination compensation using imaging condition (10).

ACKNOWLEDGEMENTS

This work was supported in part by CNPq, FAPESP, CAPES, as well as Petrobras and the sponsors of the Wave Inversion Technology (WIT) Consortium.

REFERENCES

- Billette, F., Begat, S. L., Podvin, P., and Lambare, G. (2003). Practical aspects and applications of 2d stereotomography. *Geophysics*, 68(3):1008–1021.
- Biondi, B. (2006). *3D seismic imaging*. Society of Exploration Geophysicists.

- Bleistein, N. (1986). Two-and-one-half dimensional in-plane wave propagation. *Geophysical Prospecting*, 34:686–703.
- Chattopadhyay, S. and McMechan, G. A. (2008). Imaging conditions for prestack reverse-time migration. *geo*, 73(3):S81–S89.
- Claerbout, J. (1985). *Imaging the earth's interior*. Blackwell Scientific Publications.
- Costa, J., Novais, A., Neto, F. S., and Tygel, M. (2005). 2.5D acoustic finite-difference modeling in variable density media. *Journal of Seismic Exploration*, 13:323–335.
- Costa, J. C., Neto, F. A. S., Alcântara, M. R. M., Schleicher, J., and Novais, A. (2009). Obliquity-correction imaging condition for reverse time migration. *Geophysics*, 74(3):S57–S66.
- Haney, M. M., Bartel, L. C., Aldridge, D. F., and Symons, N. P. (2005). Insight into the output of reverse-time migration: What do amplitudes mean? In *SEG International Annual Meeting, Expanded Abstracts*, pages 1950–1953.
- Kaelin, B. and Guitton, A. (2006). Imaging condition for reverse time migration. In *SEG International Annual Meeting, Expanded Abstracts*, pages 2594–2597.
- Novais, A. and Santos, L. (2005). 2.5D finite-difference solution of the acoustic wave equation. *Geophysical Prospecting*, 53:523–531.
- Valenciano, A. and Biondi, B. (2003). 2-D deconvolution imaging condition for shot-profile migration. In *SEG International Annual Meeting, Expanded Abstracts*, pages 2431–2433.